Effect of wafer bow on electrostatic chucking and back side gas cooling

Daniel L. Goodman[a)]
Nexx Systems Inc., Billerica, Massachusetts 01821-3929, USA

(Received 26 August 2008; accepted 3 November 2008; published online 16 December 2008)

Electrostatic chucks (ESCs) are used in the semiconductor industry to clamp wafers to a pedestal and combined with back side gas (BSG) cooling to control temperature during processing. The effect of wafer bow in an ESC/BSG system is studied theoretically and experimentally. An equilibrium model is developed that predicts the maximum allowed bow for initial chucking and the maximum BSG pressure once the wafer is chucked. Experimental chucking and BSG pressure data show the maximum initial bow that can be chucked agree with model predictions. Hysteresis in pressure versus flow data is also consistent with the model. The model does not predict some features of thin wafers with highly stressed films. However, deviations between the model and data in this nonlinear regime are expected. By combining the theory with the experimental data, a method to determine a safe BSG/ESC operating range is given. © *2008 American Institute of Physics*.
[DOI: 10.1063/1.3043843]

I. INTRODUCTION

Temperature control of semiconductor wafers during processing is critical to maintain device characteristics and to control deposited film stresses. Electrostatic chucking (ESC) with back side gas (BSG) cooling is often used to control temperature during processing.[1,2] These systems have traditionally been designed assuming wafers are flat before and during processing. However, wafers are often bowed due to previous processing steps, or become bowed during processing due to induced stresses. Bowed wafers are more difficult to initially chuck, and also dechuck at lower back side pressures than flat wafers. Wafer bow thus is a limiting factor in active cooling using an ESC/BSG system.

The semiconductor industry has historically used silicon wafers with thickness in the range of 600–800 μm. These full-thickness wafers can become moderately bowed due to stress in the deposited layers of metal and dielectric used in the integrated circuit manufacturing process. Excessively bowed wafers are difficult to handle robotically as well as to process. The maximum allowed initial bow is thus one of the specifications for each processing step.

Semiconductor wafers have historically been thinned after processing but before the final dicing and packaging operations. Demand for memory and smart cards, portable communication devices, and portable computers to become smaller with higher performance are forcing manufacturers to work with thinned wafers in earlier processing steps. Wafers thinned to 100–300 μm are easily bowed, either by the thinning process itself or from deposited film stresses. A stress relief step is typically used at the end of the thinning process to remove the damaged surface layer and minimize this stress and the resultant wafer bow, but some bow remains. Deposited film stresses are either intrinsic, due to lattice structure, or thermal, due to the mismatch in the coefficient of thermal expansion between the substrate and the film.

This paper analyzes the behavior of bowed wafers with ESC/BSG. We find that our modeling accurately predicts the system dynamics and the allowed processing conditions over a wide range of wafer diameters and thicknesses. We have found these results useful to interpret complex system behavior, to improve ESC/BSG system design, and to predict the range of allowed initial and in-process wafer bows.

II. EQUILIBRIUM MODEL

A bowed wafer and an ESC with integrated BSG capability are shown in Fig. 1. The wafer is assumed axially symmetric, with radius L, substrate thickness h_s, and deposited thin film thickness h_f. In the small bow limit ($B \ll L$), a geometric expansion gives the magnitude of the wafer bow as $B = L^2/2\kappa$, where κ is the wafer radius of curvature. The distance between the wafer and the ESC is $w(r,B)$, where r is the radial dimension and the minimum value of $w(r,B)$ is the gap h. The equilibrium shape of a wafer with tensile stress is cup shaped with the minimum gap at the center: $w(0,B)=h$. Wafers with compressive stress form a domed shape, with the minimum gap at the edge: $w(L,B)=h$.

A classic ESC consists of an electrode charged to a voltage V, and an insulating dielectric of thickness d and dielec-

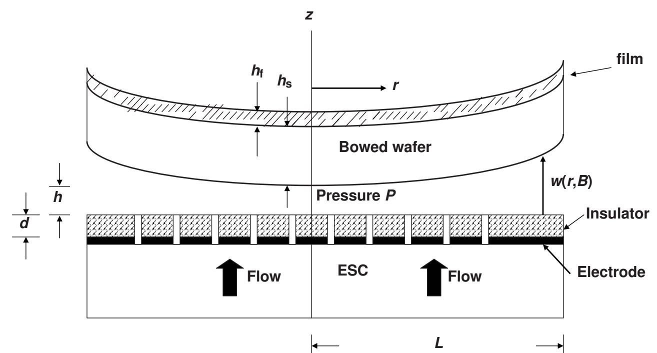

FIG. 1. The model system of ESC with bowed wafer.

a)Electronic mail: Daniel_Goodman@nexxsystems.com.

 © 2008 American Institute of Physics

Author complimentary copy. Redistribution subject to AIP license or copyright, see http://jap.aip.org/jap/copyright.jsp

tric constant k. Gas is directed to the back side of the wafer via holes in the ESC, producing a BSG pressure P.

The system energy density of the ESC and bowed wafer consists of the following four terms:

$$U = U_\sigma + U_E + U_P + U_g. \tag{1}$$

The first term, U_σ, is the elastic strain energy due to lattice mismatch strain in the substrate produced during manufacture or to thin film stresses in the film-substrate system. Thin film stresses are either intrinsic, dependent on deposition parameters, or caused by differences in the thermal expansion coefficient between the film and substrate. The second term $U_E = \varepsilon_0 \int E^2 dV/2$ is the electric field energy of the charged ESC integrated over the region between the electrode and the wafer. This volume includes both the insulator and the gap regions. The third term $U_P = \int P(B) dV$ is the energy density of the BSG pressure P in the region between the ESC and the wafer. The final term is the gravitational wafer energy $U_g = mg\bar{w}$, where m is the wafer mass and $\bar{w}$ is the average displacement. This is the smallest of the four terms, and can be neglected except for a large gap.

A. Elastic strain energy

The relationship between mismatch strain and wafer bow was first derived by Stoney[3] for the case of thin films bonded to thick substrates. Freund *et al.*[4] extended the Stoney formula to thin substrates or large deformations. We make the same assumptions as Freund *et al.*, namely, (i) the film and substrate thicknesses are small compared to the lateral dimensions, (ii) the substrate material is homogeneous, isotropic, and linearly elastic, and the film material is isotropic, and (iii) edge effects and stress components in the thickness direction **Z** can be neglected.

For the bowed wafer shown in Fig. 1, with elastic modulus E, Poisson ratio ν, substrate biaxial modulus $E_s/(1-\nu)$, and elastic strain components ε_{rr} and $\varepsilon_{\theta\theta}$, the elastic strain energy density is[4]

$$U(r,z) = \frac{E_s}{2(1-\nu^2)}[\varepsilon_{rr}(r,z)^2 + \varepsilon_{\theta\theta}(r,z)^2 + 2\nu\varepsilon_{rr}(r,z)\varepsilon_{\theta\theta}(r,z)]. \tag{2}$$

For small deflections, the strain components are related to the displacement $w(r,B)$ by

$$\varepsilon_{rr} = -zw''(r,B) + \varepsilon_m, \quad \varepsilon_{\theta\theta} = -zw'(r,B)/r + \varepsilon_m, \tag{3}$$

where $\varepsilon_m = (a_s - a_f)/a_f$ is the mismatch strain, and a_s and a_f are the substrate and film lattice parameters in an epitaxial system, respectively. This simplifies Eq. (2), which can be integrated over the wafer volume of Fig. 1 to obtain the elastic energy

$$U_\sigma = \frac{-E_s}{(1-\upsilon)} \int_0^L \int_{-hs/2}^{hs/2+hf} 2\pi r \varepsilon_{rr}^2(r,z) dz dr. \tag{4}$$

The displacements for a wafer with film in tension $w_T(r,B)$ or compression $w_C(r,B)$ are

$$w_T(r,B) = h + Br^2/L^2, \quad w_C(r,B) = h + B(1 - r^2/L^2), \tag{5}$$

and the average wafer displacement is the same for either case,

$$\bar{w}(B) = \int w(r,B) 2\pi r dr = h + B/2. \tag{6}$$

Combining Eqs. (3)–(5), and noting that w'' is the same for films in either tension or compression, the elastic strain energy is

$$U_\sigma(B) = \frac{\pi E_s}{(1-\nu)}\left[\frac{B^2 h_s^3}{3L^2} - 2B\varepsilon_m h_s h_f\right]. \tag{7}$$

Before application of an electric field, the equilibrium initial bow B_0 is the solution to

$$\frac{dU_\sigma}{dB} = \frac{2\pi E_s h_s^3}{(1-\nu)3L^2}(B - B_0) = 0, \tag{8}$$

$$B_0 = 3\varepsilon_m h_f L^2/h_s^2. \tag{9}$$

Equation (9) recovers the Stoney formula relating curvature κ to mismatch stress[3]

$$\kappa = 6\varepsilon_m h_f/h_s^2. \tag{10}$$

B. Electrostatic field energy

The electric field for the system in Fig. 1 is primarily in the axial (Z) direction. Neglecting the radial field and edge effects, the electric field is

$$E_z(r,B) = \frac{V}{w(r,B) + d/k} \tag{11}$$

and the electric field energy is

$$U_E(B) = \varepsilon_0 \pi V^2 \int_0^L \frac{r dr}{w(r,B) + d/k}. \tag{12}$$

Substituting the tensile displacement from Eq. (5) into Eq. (12), and defining the effective ESC gap $G = h + d/k$, the electric field energy is

$$U_E^T(B) = \frac{\varepsilon_0 f \pi V^2 L^2}{2B} \ln(1 + B/G), \tag{13}$$

where f is the fraction of the ESC surface covered by the electrode. A similar expression exists for the compressive electric field energy $U_E^C(B)$. For either tensile or compressive energies, the derivative dU_E/dB is

$$\frac{dU_E(B)}{dB} = \frac{\varepsilon_0 f \pi V^2 L^2}{2BG} F(B/G), \tag{14}$$

where the function $F(x) = x^{-1}\ln(1+x) - (1+x)^{-1}$.

The ESC pressure (for fixed ESC gap) is

$$P_E = dU_E/d\bar{w} = \frac{1}{\pi L^2}\frac{dU_E/dB}{d\bar{w}/dB}. \tag{15}$$

For small bow, the limiting value of $F(x) \approx x/2$. Substituting Eqs. (6) and (14) into Eq. (15), in the small bow limit, the ESC pressure is

Author complimentary copy. Redistribution subject to AIP license or copyright, see http://jap.aip.org/jap/copyright.jsp

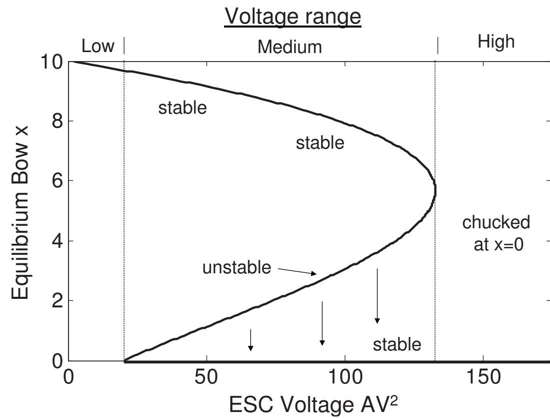

FIG. 2. Equilibrium bow before application of BSG pressure.

$$P_E = \tfrac{1}{2} f \varepsilon_0 V^2 / G^2. \tag{16}$$

This is the well-known expression for the ESC chucking pressure for a flat wafer.

C. Back side gas energy

The BSG pressure is assumed constant over the wafer surface. The energy due to this pressure P is

$$U_P = \int_0^L P w(r,B) 2\pi r dr. \tag{17}$$

The energies for either the compressive and tensile bow shape is

$$U_p(B) = \pi L^2 P(h + B/2) \tag{18}$$

and the derivative is

$$dU_P(B)/dB = \pi L^2 P/2. \tag{19}$$

The wafer bow in equilibrium satisfies $dU(B)/dB=0$. Combining Eqs. (6), (8), (14), and (19), and using the definition of the initial wafer bow B_0 from Eq. (9), the equilibrium bow is the solution to the equation

$$\frac{2E_s h_s^3}{3(1-\nu)L^2}(B - B_0) + \frac{\varepsilon_0 f V^2 L^2}{2BG} F(B/G) + L^2 P/2 - mg/(2\pi) = 0. \tag{20}$$

The first step in using the ESC/BSG system is to place the wafer onto the chuck and charge the electrode to voltage V. In this case $P=0$, and (neglecting gravity) Eq. (20) can be written as

$$H(x,x_0) = \frac{(x_0 - x)x}{F(x)} = AV^2, \tag{21}$$

where the normalized initial and equilibrium bows are $x_0 = B_0/G$, $x = B/G$, and the proportionality constant is

$$A = \frac{3\varepsilon_0 f L^4 (1-\nu)}{4E_s h_s^3 G^3}. \tag{22}$$

The equilibrium displacement as a function of applied voltage is the solution of $H(x,x_0)$ for x and shown in Fig. 2 for a typical initial bow ($x_0=10$). Three regions are identified in the figure. At low ESC charging voltage, there is only one solution to Eq. (21), and the equilibrium bow is close to the initial bow. At high ESC voltages, the ESC force exceeds the elastic bow restoring force, and the wafer is held flat with $x=0$. At intermediate ESC voltage there are two solutions to Eq. (21) for a given charging voltage. This is because the electrostatic force has a quadratic dependence on bow whereas the elastic restoring force varies only linearly.

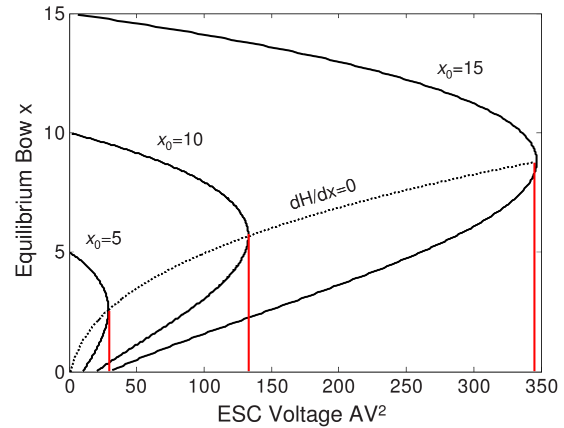

FIG. 3. (Color online) Equilibrium bow before application of BSG pressure for three values of initial bow.

If a wafer is placed on a chuck charged to an intermediate voltage, it will have an equilibrium bow on the poorly chucked upper branch. However, if the wafer is flattened by other means (such as by applying vacuum between the wafer and the ESC), the electrostatic force will overcome the elastic bow and the wafer will become well-chucked with $x=0$. The lower branch is an unstable solution to Eq. (21) and a full dynamic (as opposed to a static) treatment would show that the ESC flattens the wafer. This effect is indicated by the downward arrows drawn to the stable solution at $x=0$.

Figure 3 shows the equilibrium bow before application of BSG for three values of initial bow ($B_0=5$, 10, and 15). Also shown is the function $dH/dx=0$, which connects the maxima of each equilibrium bow curve. For each equilibrium bow, x_0, this curve gives the voltage at the transition between the medium- and high-voltage regions defined in Fig. 2. The $dH/dx=0$ curve can be plotted versus wafer diameter and thickness to find the minimum ESC voltage to chuck a bowed wafer, or equivalently the maximum allowed initial bow for a given ESC voltage.

The three vertical lines drawn in the figure illustrate the use of Fig. 3 to find the minimum initial bow x_{0m}. The leftmost line shows that for a normalized ESC voltage $AV^2=35$, the maximum initial normalized bow is $x_{0m}=5$, and the chucked equilibrium bow for this combination is approximately $x=2.5$. For a normalized ESC voltage $AV^2=135$, the maximum initial bow is $x_{0m}=10$, and the equilibrium bow for this combination is approximately $x=5$. For a normalized ESC voltage $AV^2=340$, the maximum initial bow is $x_{0m}=15$ and the equilibrium bow for this combination is $x=8.5$. Note that the equilibrium bow is approximately half the maximum initial bow. Using this approximation together with the curve labeled $dH/dx=0$ allows an estimate of maximum initial bow as a function of normalized ESC voltage.

Author complimentary copy. Redistribution subject to AIP license or copyright, see http://jap.aip.org/jap/copyright.jsp

TABLE I. Bowed wafers dimensions used for ESC and BSG experiments.

No.	Diameter (mm)	Thickness (μm)	Curvature (m)	Bow (μm)	Bow X_0
1	150	645	9–90	30–300	1–10
2	150	200	1.6–16	175–1750	5–50
3	200	735	10–1000	5–500	0.2–20
4	200	175–200	3–50	100–1700	3–50
5	300	770	14–150	75–800	2–25
6	300	200	4–100	100–2500	3–75

Once the wafer is chucked, gas is allowed to enter the BSG system and a back side pressure P established. For nonzero pressure, and neglecting gravity, Eq. (20) can be written as

$$H(x,x_0) = AV^2 - \frac{Px}{P_0F(x)}, \tag{23}$$

where $H(x,x_0)$ and A are defined in Eqs. (21) and (22), and

$$P_0 = \frac{4GE_sh_s^3}{3(1-\nu)L^4}. \tag{24}$$

Equation (23) shows that the BSG pressure reduces the ESC chucking force by a bow-dependent amount. When the pressure exceeds a threshold, the system moves from the well-chucked high-voltage regime to an intermediate regime where the behavior is more complex, and both well-chucked and poorly chucked solutions are possible.

For a well-chucked system with $x=0$, using the limiting value of $F(x)\sim x/2$ and the definition of the ESC chucking pressure from Eq. (16), Eq. (23) can be written in a simple linear form

$$P_E - P = x_0P_0. \tag{25}$$

This shows that finite initial bow is equivalent to either a reduction in ESC chucking force or an increase in BSG pressure.

III. ESC AND BSG MEASUREMENTS

A. Experimental setup

ESC experiments were performed on six sizes of bowed wafers listed in Table I. The full-thickness wafers (Nos. 1, 3, and 5) conformed to SEMI specifications.[5] Thin wafers (Nos. 2, 4, and 6) were prepared by backgrinding of wafers of types 1, 3, and 5. Full-thickness and thinned wafers were bowed by depositing stressed NiV or TiW films of thickness 0.1–2.0 μm. Metal films were deposited using a Nimbus physical vapor deposition (PVD) tool made by NEXX Systems of Billerica, MA. Background gas pressure and wafer cooling are typically adjusted to minimize film stress. However in this study, parameters were adjusted to maximize the film stress in order to create highly bowed wafers. TiW films were deposited at low background argon gas pressure ($\sim$3 mTorr) to induce high intrinsic compressive stresses. NiV films were deposited at high background argon gas pressure ($\sim$12 mTorr) to induce high intrinsic tensile stresses. In some cases, wafers were processed without cooling to add thermal mismatch stress. Pre- and postdeposition wafer curvature and film stress were measured using a Flexus stress analyzer. The Flexus uses a dual-wavelength laser interferometer to measure wafer height along a chord, which it then uses to calculate a best-fit wafer curvature κ. Table I lists these curvatures, the associated bow, and the normalized initial bow $x_0=B_0/G$.

Converting to normalized bow requires knowledge of the effective ESC gap $G=h+d/k$. The ESCs used in this study are of a classic type and have an effective gap of 32 μm. This value was first predicted from the geometry and then verified by measuring the maximum BSG pressure P_E for an unbowed wafer and solving for G using Eq. (16),

$$G = (f\varepsilon_0V^2/2P_E)^{0.5}. \tag{26}$$

ESC and BSG cooling measurements were also performed using the Nimbus sputter tool. The Nimbus contains pallet trays to transport wafers at high throughput through the vacuum processing modules. Each tray can transport 2–4 wafers depending on wafer size. For processes which require cooling, the tray contains bipolar polyimide ESCs, which are powered by charged capacitors incorporated into the tray base. Therefore each tray also contains 2–4 ESCs that are transported through the system.

The system simultaneously deposits films on 2–4 wafers depending on wafer size, which are scanned under the sputtering source to improve film uniformity. This concept, including the BSG feed and pressure measuring system is shown in Fig. 4. Gas flow measurement was performed using an MKS model 1179A mass flow controller (MFC). Back side pressure was measured using an MKS model 627 capacitance monometer. In some cases an MKS model 649

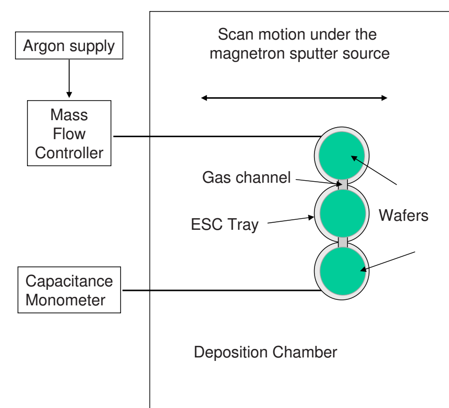

FIG. 4. (Color online) Experimental setup for ESC/BSG measurements.

Author complimentary copy. Redistribution subject to AIP license or copyright, see http://jap.aip.org/jap/copyright.jsp

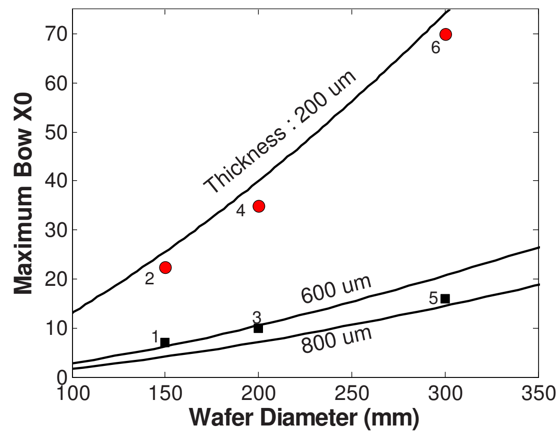

FIG. 5. (Color online) Comparison of measured and predicted maximum wafer bow. Data points are numbered to identify wafer size as listed in Table I.

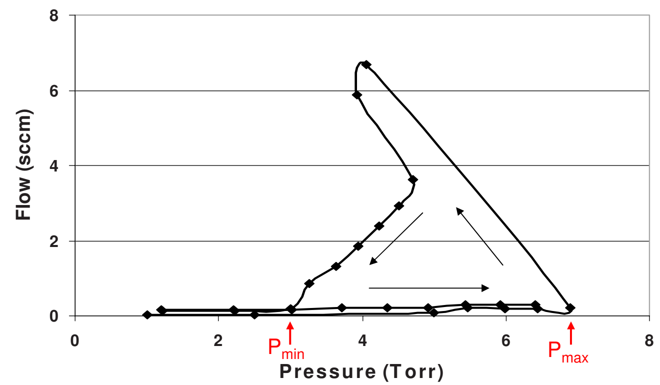

FIG. 6. (Color online) Flow vs BSG pressure for a bowed wafer. Wafer parameters are 200 mm diameter, 175 μm thickness, and 1.6 mm bow.

combined flow/pressure controller was used to take the place of the separate MFC and monometer. During normal processing, the BSG system provides pressure to 2–4 wafers simultaneously. However, the measurements described below were made using just one wafer and one ESC at a time, with the other ESCs disabled. This was done to minimize scatter in the data due to wafer variability.

B. Experimental results

The first step using a ESC/BSG system is to place the wafer onto the chuck and charge the ESC electrode to voltage V. Figure 5 shows the maximum wafer bow that can be chucked in this initial (pre-BSG) step by a voltage of ± 600 V for the Nimbus bipolar ESC. The experimental data points are labeled according to the wafer sizes listed in Table I. The data points show the initial bow above which the wafer does not chuck. For bows above this value the wafer floats on a cushion of gas, and application of ESC voltage has no effect on BSG pressure.

The three curves shown in Fig. 5 are the predicted maximum wafer bow that can be chucked at an ESC voltage of ± 600 V for thin (200 μm) and full-thickness (600–800 μm) wafers. These curves are calculated from Eq. (21) and correspond to the threshold between the medium and high-voltage regions shown in Fig. 2. The experimental data show good agreement with theory over the full range of wafer sizes listed in Table I.

Figure 6 shows a typical BSG flow versus pressure curve for a bowed wafer. The curve was obtained by slowly varying the BSG pressure so that the system was always in equilibrium. At low pressures ($P < P_{min}$) ESC chucking holds the wafer in place and the BSG flow increases approximately linearly with pressure. There is a pressure threshold, labeled P_{max} in the figure, at which the BSG pressure together with the elastic bow force exactly balances the ESC chucking force. If the back side pressure is increased above P_{max}, the wafer lifts off the ESC, gas is released, and a new equilibrium is established at higher flow and lower pressure. In order to re-establish the original equilibrium the pressure must be reduced below P_{min}. In the intermediate pressure regime ($P_{min} < P < P_{max}$) we see two possible combinations of pressure and flow. The low flow equilibrium is well chucked and the high flow equilibrium is poorly chucked.

We can understand this result as an extension of Fig. 2 to include finite BSG pressure. Figure 2 shows that at intermediate ESC voltages there are two equilibrium solutions for bow. Equation (25) shows that addition of BSG pressure is equivalent to a bow-dependent reduction in ESC voltage. Thus it seems reasonable that at finite BSG pressure there would be two equilibrium bow solutions. In fact, the equilibrium bow solution to Eq. (23) can be graphed versus initial bow and BSG gas pressure for a set ESC voltage. These three-dimensional curves are generalizations of the curve shown in Fig. 2, showing various combinations of x_0 and P, which lead to a particular equilibrium bow. Although it is satisfying to explain this intermediate two-solution regime, in practice, users will prefer to stay well within the high-voltage well-chucked regime, which has only one, fully chucked equilibrium solution.

Figure 7 shows an asymmetry in flow versus BSG pressure for a compressive (domed) wafer and a tensile (cupped) 200 mm diameter 175 μm thick wafer. The two curves are for exactly the same initial 1 mm bow. To ensure this, the curves in Fig. 7 were measured with the same wafer, first in tension, with film side up, and then subsequently in compression, with the film side down. We find that both P_{min} and P_{max} for a wafer in tension are greater than for a wafer in compression. This result is independent of wafer size or

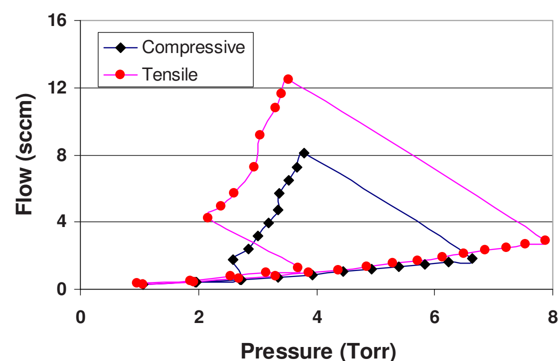

FIG. 7. (Color online) Flow vs background pressure for a single wafer shown with either compressive or tensile stresses. Wafer parameters are 200 mm diameter, 175 μm thickness, and 1.0 mm bow.

Author complimentary copy. Redistribution subject to AIP license or copyright, see http://jap.aip.org/jap/copyright.jsp

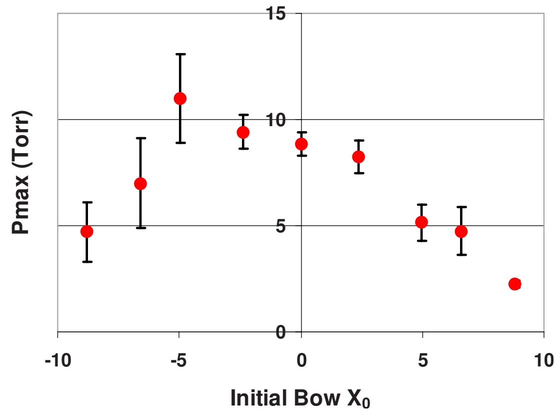

FIG. 8. (Color online) Maximum BSG pressure vs initial bow for full-thickness (645 μm) 150 mm diameter wafers.

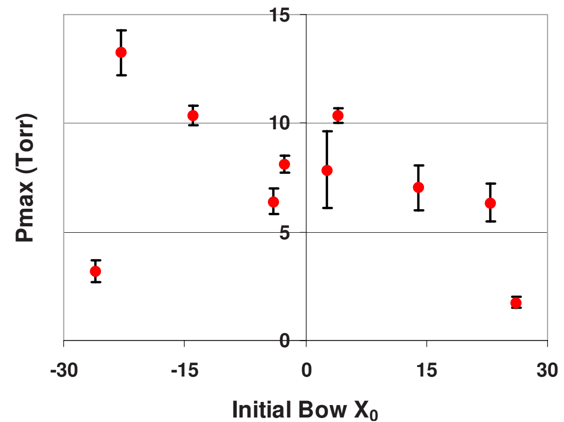

FIG. 9. (Color online) Maximum BSG pressure vs initial bow for thin (200 μm) 150 mm diameter wafers.

thickness. The difference between compressive and tensile pressure values is greatest for thin wafers and for wafers with large bows.

This asymmetry would not be expected from the linear theory presented in Sec. I. Although the tensile and compressive strain energies $U_E^T(B)$ and $U_E^C(B)$ are not equal, their derivatives with respect to bow in Eq. (14) *are* equal. Since it is the derivative that determines force balance and equilibrium, the theory does not predict the observed asymmetry.

Explanations for the asymmetry relate to the dynamic response of tensile and compressive wafers to a BSG overpressure event. Figure 1 shows a tensile wafer with back side pressure. As the gas pressure behind a tensile wafer builds, the edges tend to roll up, allowing the gas to escape and re-establishing a chucked equilibrium. For a compressive wafer, it is the wafer edges that are in closest contact with the ESC. Lifting the edges of the wafer to allow a burst of gas to escape would significantly reduce the area of the wafer in contact with the ESC and more easily lead to a transition to an unchucked equilibrium. This concept could be modeled by adding conductance and flow to the pressure term Eq. (19), and solving the time-dependent dynamics. However, that calculation is beyond the scope of this paper.

Another explanation is related to local asymmetries. The strain energy given in Eq. (3) assumes small axisymmetric displacements. However, displacements at large BSG pressure can be localized in one area, rather than axisymmetric. This is especially true for thin wafers, which are not rigid or self-supporting. We have observed thin wafers flexing in one area to discharge an overpressure gas burst. Modeling this effect requires off-diagonal terms in the strain energy Eq. (2) and more complicated deflection terms in Eq. (3). This calculation is also beyond the scope of this paper.

Figure 8 shows $P_{\max}$ versus initial bow x_0 for full-thickness 150 mm wafers (wafer size 1), where $P_{\max}$ is maximum BSG pressure as defined in Fig. 6. The figure shows that wafers in tension ($x_0 < 0$) are able to support higher BSG pressure than wafers in compression ($x_0 > 0$). For the 150 mm wafers, the wafers in tension are even able to maintain higher BSG pressures than wafers with initial neutral stress. This suggests that maintaining a slightly tensile stress during processing with ESC/BSG may be beneficial, and provide additional safety margin against ESC dechucking.

Wafers with large tensile bows tend to have larger error bars than wafers with neutral or compressive stress. A portion of this scatter is due to complex system dynamics. Another portion is due to residual electrostatic charges initially on the polyimide ESC or on the wafer, or created in the BSG system by collisions with the walls and carried onto the wafer by the flowing gas. ESC systems with polyimide chucks regularly reverse polarity to prevent the polyimide surface from becoming polarized. This reversal will tend to either increase or decrease $P_{\max}$, depending on the sign and position of the residual charges. Careful charge neutralization during the experiments reduced this effect for all wafers, but did not eliminate large scatter for tensile wafers.

Figure 9 shows $P_{\max}$ versus initial bow x_0 for thin 150 mm wafers (wafer size 2). Note the increased asymmetry between initial tensile and compressive bows. Note also that the scale is three times larger, showing the larger range of initial bows which may be chucked. For the same induced stress, thin wafers bow more than thick wafers, but they also are easier to chuck for the same bow because they have smaller restoring force. The predicted cubic scaling with thickness can be seen from Eq. (24).

Figures 10 and 11 show $P_{\max}$ versus initial bow x_0 for full-thickness 200 and 300 mm wafers (wafer sizes 3 and 5). The asymmetry between tensile and compressive bowed wa-

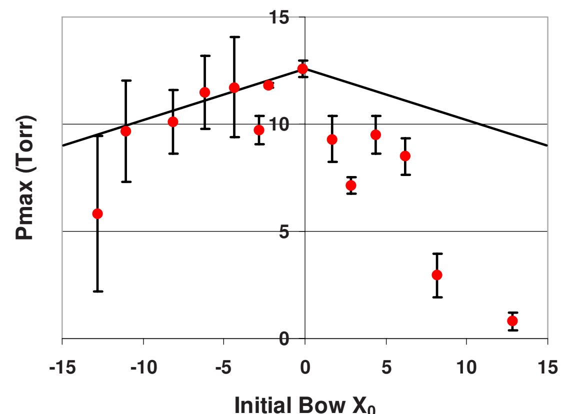

FIG. 10. (Color online) Maximum BSG pressure vs initial bow for full-thickness (735 μm) 200 mm diameter wafers. Also shown is the predicted maximum BSG pressure curve from Eq. (25).

Author complimentary copy. Redistribution subject to AIP license or copyright, see http://jap.aip.org/jap/copyright.jsp

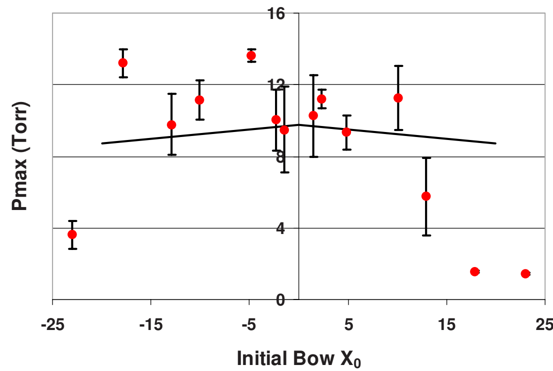

FIG. 11. (Color online) Maximum BSG pressure vs initial bow for full-thickness (770 μm) 300 mm diameter wafers. Also shown is the predicted maximum BSG pressure curve from Eq. (25).

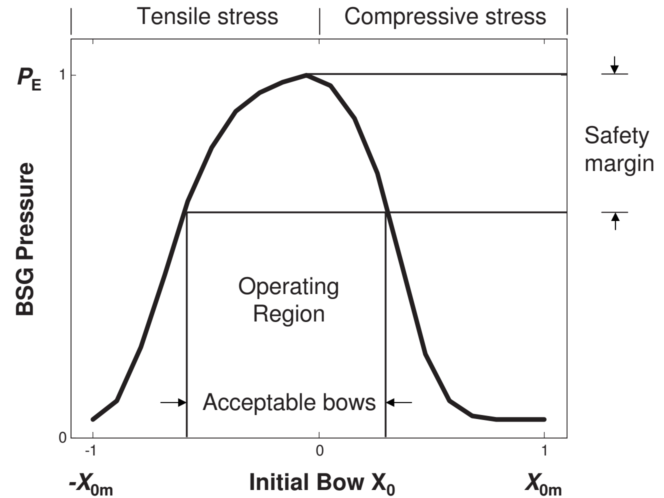

FIG. 12. The safe operating region for BSG pressure as a function of initial bow x_0 and ESC pressure P_E.

fers can again be seen, with the falloff in P_{max} with bow approximately twice as fast for compressive as for tensile-stressed wafers in both cases.

Also shown in the figures are linear scaling for P_{max} versus x_0 calculated from Eq. (25). Since the system is well chucked with $x \sim 0$, we are justified in using the small x linearized Eq. (25) rather than the full Eq. (23). In Fig. 10, the predicted slope agrees with the data for tensile bows, but underestimates the steepness of the falloff in P_{max} for compressive bows. In Fig. 11 agreement between theory and experiment is difficult to determine for small bows due to large error bars, but the measured BSG pressure clearly falls off faster than predicted at large bow.

C. Application to wafer processing

The model together with the data in Figs. 8–11 can be used to aid the design of ESC/BSG processes when used with bowed wafers. The tool user typically wishes to maximize process throughput while holding the wafers below a device-dependent temperature. The throughput will be limited by the back side cooling rate, which is approximately proportional to the BSG pressure for typical BSG pressures.[6] The BSG pressure is regulated at a value less than the theoretical maximum to ensure reliable operation. If the range of wafer bows is significant, then the BSG pressure must be further derated compared to the value used for unbowed wafers. The following steps allow an estimate of the safe operating pressure for a given range of bows, or can be used to create a specification for acceptable incoming bows, in order to provide the required cooling, given particular ESC/BSG parameters.

(1) Find the effective ESC gap G and the normalized ESC voltage AV^2. The gap is found by measuring the maximum BSG pressure P_E using flat wafers and then substituting into Eq. (26). Once G is known, the normalized ESC voltage is found from Eq. (22).

(2) Using either Eq. (21) or Fig. 3, determine the maximum bow x_{0m} that can be chucked for the normalized ESC voltage of step 1. If Fig. 3 is used, one first finds the value on the curve marked dH/dX corresponding to the normalized ESC voltage. The maximum bow x_{0m} that can be chucked is approximately twice this equilibrium x value.

(3) Draw a curve with center value P_E (from step 1) and half width x_{0m} (from step 2), using the shapes of Figs. 8–11 as a guide. It is useful to label the axes with both bow and stress, with the stress values calculated from the Stoney formula [Eq. (9)]. An example curve is shown in Fig. 12.

(4) Determine the induced process stress. The user will likely have previous process experience with the recipe of interest using flat wafers. For single-step processes, the induced process stress can be determined by measuring the film stress after processing. Some recipes contain multiple steps, whereby steps with compressive and tensile stresses are alternated to control wafer bow. For such a multistep recipe, the maximum stress during processing may exceed the final stress. In that case the maximum value needs to be estimated by measuring the effect of each step separately.

(5) Combine the range of bow stresses and the induced process stress, and convert to a range of normalized bow. Then decide on a reasonable pressure safety margin, as shown in Fig. 12. The purpose of the safety margin is to guarantee good chucking and full cooling even if some residual charge remains on the ESC surface. Finally, use the area marked "operating region" to determine either the acceptable range of initial bows given an operating BSG pressure P_E, or to determine P_E (and therefore the ESC operating voltage) given the range of initial bows.

D. Application to Johnsen–Rebek electrostatic chucks

There are two types of ESCs commonly used in industry: the classic ESC used in this study and the Johnsen–Rebek (JR) ESC, which uses charge migration in a dielectric to create strong electric fields at small noncontact areas with small gaps.[7] The JR chuck has recently increased in popularity, especially for cooling of demanding front-end applica-

Author complimentary copy. Redistribution subject to AIP license or copyright, see http://jap.aip.org/jap/copyright.jsp

tions. Therefore it is worth noting any experimental differences one would expect for chucking of bowed wafers with JR, rather than a classic ESC.

JR chucks have a smaller effective gap G than classic ESCs, but the equations describing the Coulomb force for the two types of chucks are identical.[8] Therefore the theory derived in this paper is applicable to either type of chuck as long as the proper effective gap is used. This gap can be measured as indicated in Sec. III A using Eq. (26).

The JR chuck is capable of higher chucking forces for the same operating voltage than the classic ESC, but is more sensitive to wafer conditions, including back side dielectric quality and thickness and doping level.[8] In practice, the classic ESC is often operated at higher voltages than the JR chuck, in order to achieve the necessary BSG pressure and wafer cooling rate.

Another difference between the two types of chuck is a reduction in the length of time that surface charge remains on the surface of a JR chuck, compared to a classic ESC. This is due to the lower surface resistivity of the JR chuck. Because of this effect, it is possible that the width of the error bars in Figs. 7–11 would be smaller if a JR rather than a classic chuck had been used in these experiments. On the other hand, the increased sensitivity of the JR chuck to wafer conditions might have added to experimental uncertainty in the maximum back side pressure versus initial bow.

The experimental work described in this paper varied the wafer bow B and the wafer diameter L while holding constant the ESC voltage V and effective ESC gap G. Although we expect our models and experimental results to be applicable to a JR ESC operating at a smaller gap G and a different voltage V, verification will require testing with the appropriate hardware.

IV. CONCLUSIONS

The effect of wafer bow on ESC and on wafer cooling using ESC with BSG has been studied theoretically and experimentally. The model extends the Stoney curvature formula to include ESC chucking and predicts the maximum allowed bow before application of BSG. Measured values agree with the model for all wafer sizes. Measured values of maximum BSG pressure versus initial bow exceed the model predictions and also show asymmetry between tensile- and compressive-stressed wafers, an unexpected result possibly due to displacements beyond linear model assumptions. Despite the limitations of the model, it can be used with experimental data to design cooling processes for the full range of bowed wafers. A method to determine a safe operating range for ESC/BSG is shown.

ACKNOWLEDGMENTS

Steven Golovato, Kathy O'Donnell, and Michael Tsuk provided helpful comments to improve this manuscript.

[1] D. R. Wright, L. Chen, P. Federlin, and K. Forbes, J. Vac. Sci. Technol. B **13**, 1910 (1995).
[2] J.-F. Daviet, L. Peccoud, and F. Mondon, J. Electrochem. Soc. **140**, 3245 (1993).
[3] G. G. Stoney, Proc. R. Soc. London, Ser. A **82**, 172 (1909).
[4] L. B. Freund, J. A. Floro, and E. Chason, Appl. Phys. Lett. **74**, 1987 (1999).
[5] "Polished Monocrystaline Silicon Wafers," Semiconductor Equipment and Materials International Standard Report No. M1-0707, 2007.
[6] R. Powell and S. Rossnagel, *PVD for Microelectronics: Sputter Deposition Applied to Semiconductor Manufacturing* (Academic, San Diego, 1999), pp. 143–147.
[7] F. A. Johnson and K. Rahbek, J. Inst. Electr. Eng. **61**, 713 (1923).
[8] S. Qin and A. McTeer, J. Appl. Phys. **102**, 064901 (2007).

Author complimentary copy. Redistribution subject to AIP license or copyright, see http://jap.aip.org/jap/copyright.jsp